LETTER

doi:10.1038/nature10013

# Interannual atmospheric variability forced by the deep equatorial Atlantic Ocean

Peter Brandt[1], Andreas Funk[1], Verena Hormann[1]†, Marcus Dengler[1], Richard J. Greatbatch[1] & John M. Toole[2]

**Climate variability in the tropical Atlantic Ocean is determined by large-scale ocean–atmosphere interactions, which particularly affect deep atmospheric convection over the ocean and surrounding continents[1]. Apart from influences from the Pacific El Niño/Southern Oscillation[2] and the North Atlantic Oscillation[3], the tropical Atlantic variability is thought to be dominated by two distinct ocean–atmosphere coupled modes of variability that are characterized by meridional[4,5] and zonal[6,7] sea-surface-temperature gradients and are mainly active on decadal and interannual timescales, respectively[8,9]. Here we report evidence that the intrinsic ocean dynamics of the deep equatorial Atlantic can also affect sea surface temperature, wind and rainfall in the tropical Atlantic region and constitutes a 4.5-yr climate cycle. Specifically, vertically alternating deep zonal jets of short vertical wavelength with a period of about 4.5 yr and amplitudes of more than 10 cm $s^{-1}$ are observed, in the deep Atlantic, to propagate their energy upwards, towards the surface[10,11]. They are linked, at the sea surface, to equatorial zonal current anomalies and eastern Atlantic temperature anomalies that have amplitudes of about 6 cm $s^{-1}$ and 0.4 °C, respectively, and are associated with distinct wind and rainfall patterns. Although deep jets are also observed in the Pacific[12] and Indian[13] oceans, only the Atlantic deep jets seem to oscillate on interannual timescales. Our knowledge of the persistence and regularity of these jets is limited by the availability of high-quality data. Despite this caveat, the oscillatory behaviour can still be used to improve predictions of sea surface temperature in the tropical Atlantic. Deep-jet generation and upward energy transmission through the Equatorial Undercurrent warrant further theoretical study.**

Tropical Atlantic variability, which modulates the seasonal migration of the intertropical convergence zone, is dominated by two modes of behaviour[8,9]. The meridional mode, peaking during boreal spring, is characterized by a north–south sea-surface-temperature (SST) gradient that drives cross-equatorial wind anomalies from the cold hemisphere to the warm[4,5]. The zonal mode is characterized by an east–west SST gradient along the Equator and is associated with marked zonal wind anomalies[6,7]. It is most pronounced during boreal summer when the seasonal maximum in equatorial upwelling leads to the development of the eastern Atlantic SST cold tongue. The zonal mode is often referred to as the Atlantic counterpart to the Pacific El Niño. The period of zonal-mode-like oscillations estimated from observations, models and theory ranges from 19 months to 4 years[6,14–16]. However, aspects of the intrinsic ocean dynamics, such as year-to-year variations in the strength of tropical instability waves, are similarly identified as causes of interannual SST variability[17] and may themselves be able to force variability in the atmosphere.

During the past 10–20 yr, the eastern equatorial Atlantic SST, represented by the ATL3 index (that is, the average SST anomaly inside the box shown in Fig. 1a), has shown pronounced variability on interannual timescales, dominated by the period range of 4–5 yr; maximum explained variance of different ocean parameters is found at a period of 1,670 d (Supplementary Fig. 1). The associated harmonic amplitude of local SST fluctuations, which is $0.29 \pm 0.08$ °C averaged over the ATL3 region, is generally high in the eastern equatorial Atlantic, with local amplitudes of up to 0.4 °C (Fig. 1a and Supplementary Fig. 2). The regression of surface winds and rainfall on the 1,670-d SST harmonic reveals that anomalous westerlies along the Equator, convergent meridional wind anomalies particularly in the western tropical Atlantic, and positive rainfall anomalies in a wide belt around the Equator are associated with positive SST anomalies.

A 1,670-d cycle is also found in the surface geostrophic zonal velocity anomaly at the Equator and is again the dominant interannual variability, with a harmonic amplitude of $5.9 \pm 1.9$ cm $s^{-1}$. Phases of eastward surface flow coincide with SST warm phases in the eastern equatorial Atlantic (Fig. 1b). Whereas the 1,670-d period stands out as the dominant interannual variability timescale of the equatorial zonal surface flow, this is not the case for the wind forcing, which instead shows more irregular fluctuations during the analysed time interval (NCEP/NCAR reanalysis wind data). Such a dominant signal in the ocean seems to contradict early model results, in which the equatorial ocean response to wind forcing with periods longer than about 150 d was found to be a succession of equilibrium responses with the strength of the flow independent of the forcing period[18]. As we show below, variability in the 4–5-yr period band is a ubiquitous feature of the equatorial Atlantic and, furthermore, is associated with upward propagation of energy in the ocean. We propose that the variability in the equatorial zonal surface flow is not due to wind forcing with the same period but rather is a mode internal to the ocean, with its origin in the abyss (perhaps as deep as several thousand metres). If this is indeed the case, then the observed atmospheric variability in the 4–5-yr period band in the equatorial Atlantic can be interpreted as a consequence of internal ocean dynamics.

Analysis of zonal velocities at 1,000-m depth as observed by Argo floats[19] reveals periodic behaviour similar to that of the SST and surface geostrophic zonal velocity anomalies (Fig. 1b). The dominant period, of 4.4 yr, in the Argo float drift data for the period 1998–2010 is in agreement with earlier estimates from moored zonal velocity observations in the depth range 600–1,800 m made during 2000–2006[11] (4.4 yr) and with the estimate from hydrographic observations made during 1972–1998[10] ($5 \pm 1$ yr). The deep velocity and density fluctuations have been dynamically described as a mixture of high-baroclinic-mode Kelvin and Rossby waves representing quasi-steady equatorial deep jets[10,11]. Such vertically alternating zonal jets with vertical wavelengths between 300 and 700 m are similarly present in the Pacific[12,20] and Indian oceans[13,21]. In the Atlantic, a downward phase velocity of equatorial deep jets (of about 100 m $yr^{-1}$) is observed[11] that corresponds, according to linear internal wave theory, to upward energy propagation. Our moored observations reveal downward phase propagation from below the Equatorial Undercurrent (EUC) at about 200-m depth to about 2,000-m depth (Fig. 2 and Supplementary Fig. 3), suggesting a deep generation mechanism for equatorial deep jets. Observed variations in the vertical phase velocity are probably due to changes in the amplitudes of different superimposed baroclinic modes, as also indicated by changes in the vertical wavelength (Fig. 2). Theories of

[1]IFM-GEOMAR, Leibniz-Institut für Meereswissenschaften an der Universität Kiel, Düsternbrooker Weg 20, 24105 Kiel, Germany. [2]Woods Hole Oceanographic Institution, Woods Hole, Massachusetts 02543, USA. †Present address: Cooperative Institute for Marine and Atmospheric Studies, University of Miami, and National Oceanic and Atmospheric Administration/Atlantic Oceanographic and Meteorological Laboratory, Miami, Florida 33149, USA.

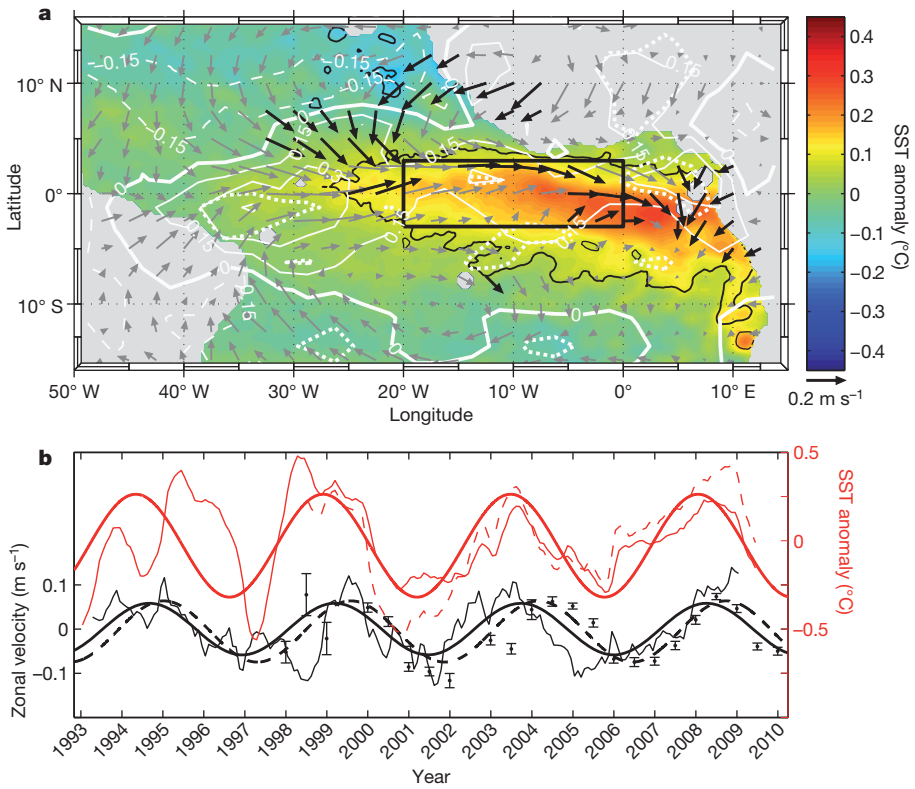


**Figure 1 | Interannual variability in the tropical Atlantic associated with a 1,670-d cycle.** **a**, Anomalies of SST (colour scale), surface wind (arrows) and rainfall (white contours: solid, positive; dashed, negative; every 0.15 mm $d^{-1}$) as determined through regression on the harmonic fit of the SST anomalies (microwave optimally interpolated SST) averaged within the marked box (ATL3: 3° S–3° N, 20° W–0°). We mark significant correlations (95%) of harmonic fit with SSTs (black lines), winds (black arrows) and rainfall (white dotted lines). **b**, ATL3 SST anomaly (microwave optimally interpolated SST, red dashed; HadISST, red thin solid) with 1,670-d harmonic fit (red thick solid), surface zonal velocity anomaly (Equator, 35° W–15° W; black thin solid) with 1,670-d harmonic fit (black thick solid), and 1,000-m zonal velocity (1° S–1° N, 35° W–15° W; black dots with standard errors) with 1,670-d harmonic fit (black thick dashed).

deep-jet generation involve instabilities associated with the propagation of intraseasonal mixed Rossby gravity waves[22,23] or the Equator-crossing deep western boundary current[24]. However, until now the proposed theories have failed to explain the observed strength and complex behaviour of the deep jets in the different ocean basins.

Propagation of deep-jet energy towards the surface is complicated by the presence of a strong, vertically-sheared mean current, the EUC, with maximum eastward velocities of more than 60 cm $s^{-1}$ at about 80-m depth (Fig. 3a). Theoretical studies indicate that the EUC effectively modifies dispersion characteristics of Kelvin and Rossby waves[25]. On seasonal timescales, the background flow partly inhibits the downward propagation of high-baroclinic-mode energy, explaining the dominance of low-baroclinic-mode seasonal waves at depth. Theoretical studies of internal wave propagation motivated by observed internal wave transmissions across an atmospheric jet suggest, however, that an energy transfer across critical levels—that is, where the horizontal phase velocity equals the background mean flow—is possible[26].

The amplitude of the 1,670-d harmonic oscillation of zonal velocity in the upper 600 m of the water column is largest in the 300–600-m depth interval (Fig. 3b), where it explains up to 60% of the variance contained in the monthly zonal velocity anomalies (Fig. 3d). Local minima in the amplitude of the 1,670-d oscillation are indicated near

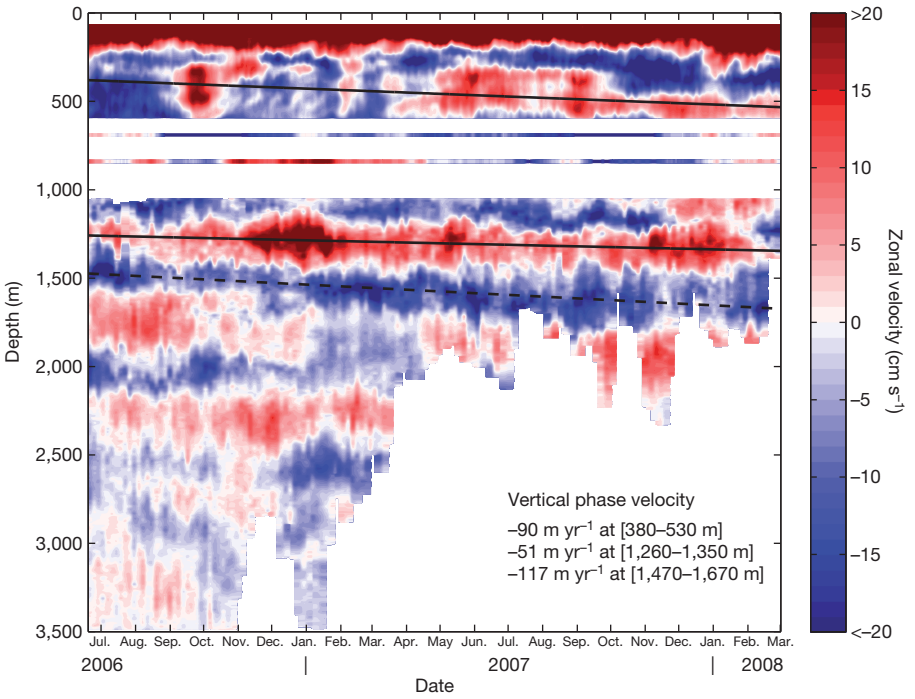


**Figure 2 | Zonal velocities at the Equator, 23° W.** Velocity data above 600 m are from a moored acoustic Doppler current profiler with annual and semi-annual cycles subtracted, those between 600 and 1,000 m are from two single-point current meters, and those below 1,000 m are from a moored profiler. The white areas mark depths not sampled by the deployed instrumentation. Linearized phase lines (eastward jets, solid; westward jet, dashed) of equatorial deep jets are calculated from about 7-yr of moored current data (above 600 m) and from the presented data (below 1,000 m). Associated vertical phase velocities are given in the figure.

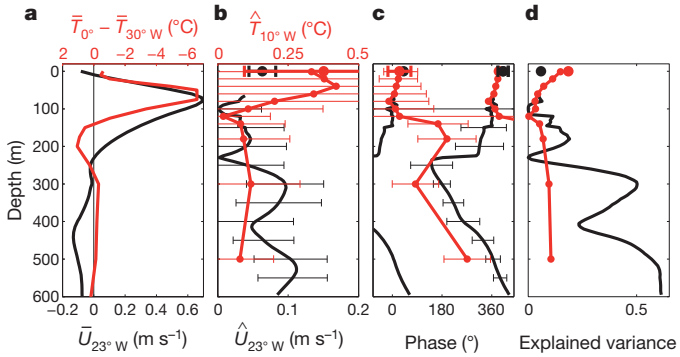


**Figure 3 | Mean zonal velocity, zonal temperature gradient and harmonic analysis of 1,670-d oscillation.** **a**, Moored mean zonal velocity ($\bar{U}$) at the Equator, 23 °W (black), and climatological[27] mean zonal temperature ($\bar{T}$) difference at the Equator between 0° and 30° W (red). **b**–**d**, 1,670-d harmonic amplitude (**b**), phase (**c**) and explained variance (**d**) of equatorial moored zonal velocities at 23° W (black curves ($\hat{U}_{23°\,W}$)), equatorial surface zonal velocity averaged between 35° W and 15° W (black dots), and subsurface temperatures (red curves ($\hat{T}_{10°\,W}$) and small red dots) and microwave optimally interpolated SST (big red dot) at the Equator, 10° W. Zero phase corresponds to 1 January 1993; explained variance is calculated using monthly mean data with the mean seasonal cycle subtracted. Information on the calculation of error bars in **b** and **c** can be found in Methods.

the core and at the lower boundary of the EUC (Fig. 3b), and amplitudes of about 6 cm s$^{-1}$ are derived at the surface. The variance explained by the 1,670-d harmonic oscillation decreases towards the surface (Fig. 3d), mainly as a result of the increasing strength of intraseasonal fluctuations. Although the vertical phase propagation is consistently downward below the EUC, the phase jumps by about 180° at the lower boundary of the EUC (Fig. 3c), approximately at the critical level for the propagation of high-baroclinic-mode equatorial Kelvin waves.

The 1,670-d fluctuations are also pronounced in subsurface temperature records. Temperatures are affected in two ways by the presence of equatorial deep jets: isopycnal displacements associated with the deep jets will lead to temperature variations that are phase-shifted in space and time relative to the velocity anomalies, depending on the character (Rossby or Kelvin) of the wave[10]; and in the presence of climatological zonal temperature gradients, zonal advection associated with the jets might induce changes in the temperature fields. For example, in-phase oscillations of surface zonal velocity and near-surface temperatures (Fig. 3c) are in agreement with the propagation of equatorial Kelvin waves; that is, eastward velocities are associated with downward isopycnal (isothermal) displacements and vice versa. A deeper thermocline could, in turn, be associated with reduced downward heat transport through diapycnal mixing causing higher SSTs. In the equatorial Atlantic, the climatological[27] zonal temperature gradient changes sign with depth, further complicating the interpretation of the observed phase structure of the subsurface temperature variability: for example, the reversal of the zonal temperature gradient with depth in the lower part of the EUC (Fig. 3a) might be responsible for the phase shift with depth of the 1,670-d harmonic oscillation of the subsurface temperature (Fig. 3c). Although the understanding of the propagation characteristics of the jets in the presence of strong mean currents and zonal tracer gradients deserves further theoretical study, these observations suggest that equatorial deep-jet energy propagates to the surface and affects sea surface conditions.

Observations in the equatorial Atlantic reveal a similar periodic behaviour for deep-jet oscillations over different time intervals and depth ranges[10,11]. Such consistent behaviour could arise from the development of high baroclinic basin modes[22] established by the eastward and westward propagation of Kelvin and Rossby waves, respectively[28]. In this case, vertical phase and energy propagation can occur only for quasi-resonant modes with active forcing and dissipation. The basin width of the Indian Ocean suggests a similar period for equatorial deep-jet oscillations as in the Atlantic, with rather different behaviour in the Pacific as a result of the much greater basin width. Argo float drift data from about 1,000-m depth represent a consistent data set that is available for all three oceans[19]. In the Atlantic, maximum

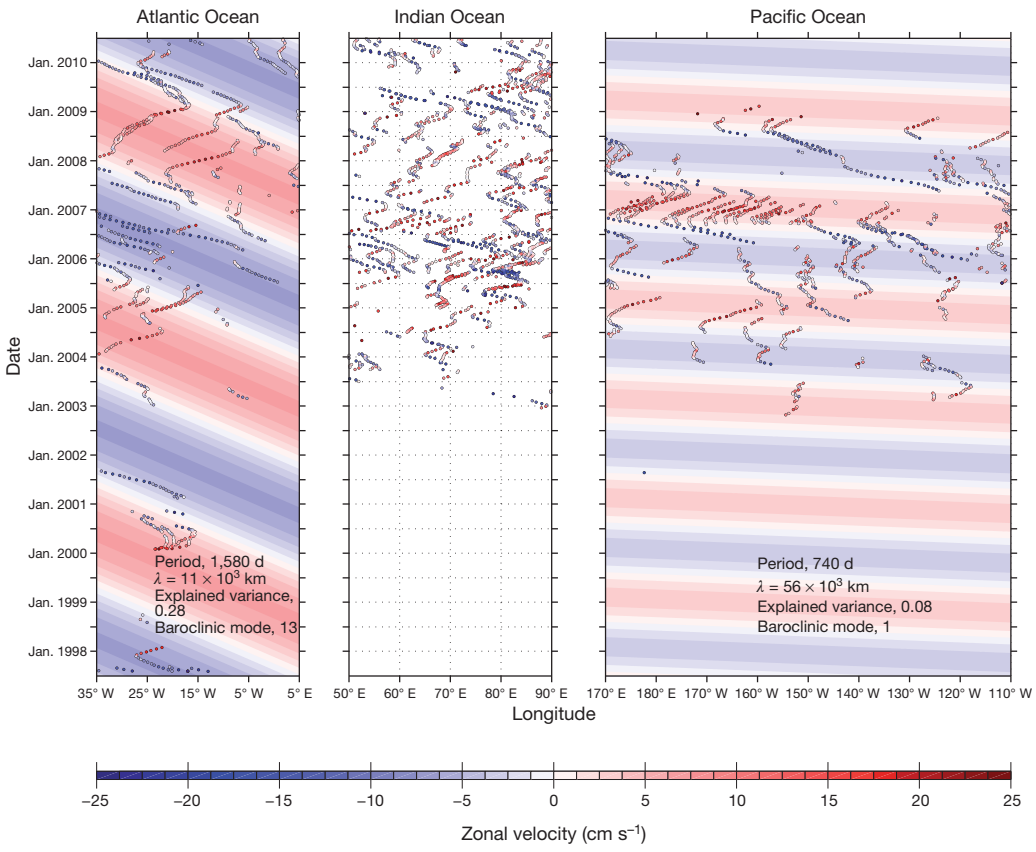


**Figure 4 | Equatorial zonal velocities from 1,000-m Argo float drift data.** Argo float drift data (coloured dots, colour scale) were acquired between latitudes 1° S and 1° N. The dominant interannual variability in the Atlantic and Pacific oceans obtained by maximizing explained variance using a plane-wave fit is visualized by colour shadings. Associated harmonic parameters for the Atlantic and Pacific oceans are given in the figure.

explained variance is found for westward-propagating Rossby waves of baroclinic mode 13 (corresponding to a vertical wavelength of about 600 m at 1,000-m depth) and a period of 1,580 d, corresponding to a zonal wavelength ($\lambda = 2\pi/|k|$, where $k$ is the zonal wavenumber) of $11 \times 10^3$ km. In the Pacific, only weak signals of high-baroclinic-mode variability were extracted from the approximately 7-yr-long time series, which could be expected as estimated deep-jet oscillation periods are in the multidecadal range[12,20]. The dominant signal there is associated with low-baroclinic-mode variability. Despite there being geometric similarities between the Indian and Atlantic oceans, during the analysed time frame the Indian Ocean Argo float velocities are characterized by incoherent signals in the interannual period range, with no preferred period (Fig. 4). From this analysis, we expect no influence of equatorial deep jets on the surface conditions in the Indian and Pacific oceans on interannual timescales.

In analysing the seasonality of the Atlantic deep-jet surface expressions, we find that the amplitude of the 1,670-d cycle of zonal velocity is seasonally independent whereas the corresponding amplitudes of the ATL3 SST anomalies at this period are instead strongest during boreal summer and November/December (Supplementary Figs 6 and 7). These periods are identified as cold seasons with shallow thermocline depths in the east and active Bjerknes positive feedback[29,30]. During boreal spring when the tropical Atlantic is uniformly warm, the influence of the 1,670-d zonal velocity anomalies on SST is weak. Such behaviour is consistent with the equatorial zonal surface flow forced by interior ocean dynamics, whereas associated SST variations are seasonally modulated. On decadal timescales, the strength and period of the deep-jet oscillations may vary over time. The modulation could be due, for example, to a change in the dominant baroclinic mode affecting the basin mode period[22,28]. Such behaviour is suggested by Supplementary Fig. 8, although other modes of variability, such as the Pacific El Niño/Southern Oscillation[2] and the North Atlantic Oscillation[3], could also be influencing the time series. Despite this caveat, the surface expressions of the deep jets can clearly be used to improve the prediction of equatorial Atlantic SST, which is crucial for seasonal to interannual climate forecasting in the region[9].

## METHODS SUMMARY

We calculated surface zonal velocity anomaly at the Equator, averaged between 35° W and 15° W (Fig. 1b), by applying a second-order fit in latitude to monthly mean meridional sea level anomaly distributions between 1° N and 1° S and evaluating equatorial geostrophy using the obtained curvature. The standard error of annual mean Argo float velocities (Fig. 1b) was calculated by dividing their standard deviation by the square root of the number of float observations. We filtered monthly time series (Fig. 1b) using a running annual mean. Harmonic analyses of zonal velocity and temperature (Figs 1b and 3) were performed by applying a linear regression model in a least-squares sense to the data. We approximated the degrees of freedom used for the calculation of the standard error of the resulting amplitudes as the length of the time series divided by a quarter of the deep-jet oscillation period. The significance of the correlation (Fig. 1a) was obtained using surface wind and rainfall time series of the same length as the microwave optimally interpolated SST with corresponding degrees of freedom. Sources and time intervals of all data sets used in this study are given in Supplementary Table 1.

**Full Methods** and any associated references are available in the online version of the paper at www.nature.com/nature.

**Received 9 November 2010; accepted 21 March 2011.**
**Published online 18 May 2011.**

1. Giannini, A., Saravanan, R. & Chang, P. Oceanic forcing of Sahel rainfall on interannual to interdecadal time scales. *Science* **302,** 1027–1030 (2003).
2. Chang, P., Fang, Y., Saravanan, R., Ji, L. & Seidel, H. The cause of the fragile relationship between the Pacific El Niño and the Atlantic Niño. *Nature* **443,** 324–328 (2006).
3. Czaja, A., van der Vaart, P. & Marshall, J. A diagnostic study of the role of remote forcing in tropical Atlantic variability. *J. Clim.* **15,** 3280–3290 (2002).
4. Carton, J. A., Cao, X., Giese, B. S. & da Silva, A. M. Decadal and interannual SST variability in the tropical Atlantic Ocean. *J. Phys. Oceanogr.* **26,** 1165–1175 (1996).
5. Chang, P., Ji, L. & Li, H. A decadal climate variation in the tropical Atlantic Ocean from thermodynamic air-sea interactions. *Nature* **385,** 516–518 (1997).
6. Zebiak, S. E. Air–sea interaction in the equatorial Atlantic region. *J. Clim.* **6,** 1567–1586 (1993).
7. Carton, J. A. & Huang, B. Warm events in the tropical Atlantic. *J. Phys. Oceanogr.* **24,** 888–903 (1994).
8. Chang, P. *et al.* Climate fluctuations of tropical coupled systems — The role of ocean dynamics. *J. Clim.* **19,** 5122–5174 (2006).
9. Kushnir, Y., Robinson, W. A., Chang, P. & Robertson, A. W. The physical basis for predicting Atlantic sector seasonal-to-interannual climate variability. *J. Clim.* **19,** 5949–5970 (2006).
10. Johnson, G. C. & Zhang, D. Structure of the Atlantic Ocean equatorial deep jets. *J. Phys. Oceanogr.* **33,** 600–609 (2003).
11. Bunge, L., Provost, C., Hua, B. L. & Kartavtseff, A. Variability at intermediate depths at the equator in the Atlantic Ocean in 2000–06: annual cycle, equatorial deep jets, and intraseasonal meridional velocity fluctuations. *J. Phys. Oceanogr.* **38,** 1794–1806 (2008).
12. Johnson, G. C., Kunze, E., McTaggart, K. E. & Moore, D. W. Temporal and spatial structure of the equatorial deep jets in the Pacific Ocean. *J. Phys. Oceanogr.* **32,** 3396–3407 (2002).
13. Luyten, J. R. & Swallow, J. C. Equatorial undercurrents. *Deep-Sea Res.* **23,** 999–1001 (1976).
14. Ruiz-Barradas, A., Carton, J. A. & Nigam, S. Structure of interannual-to-decadal climate variability in the tropical Atlantic sector. *J. Clim.* **13,** 3285–3297 (2000).
15. Wang, F. & Chang, P. A linear stability analysis of coupled tropical Atlantic variability. *J. Clim.* **21,** 2421–2436 (2008).
16. Ding, H., Keenlyside, N. S. & Latif, M. Equatorial Atlantic interannual variability: the role of heat content. *J. Geophys. Res.* **115,** C09020 (2010).
17. Jochum, M., Murtugudde, R., Malanotte-Rizzoli, P. & Busalacchi, A. in *Earth Climate: The Ocean-Atmosphere Interaction* (eds Wang, C., Xie, S.-P. & Carton, J. A.) 181–188 (Geophys. Monogr. Ser. 147, American Geophysical Union, 2004).
18. Philander, S. G. H. & Pacanowski, R. C. Response of equatorial oceans to periodic forcing. *J. Geophys. Res.* **86,** 1903–1916 (1981).
19. Lebedev, K. V., Yoshinari, H., Maximenko, N. A. & Hacker, P. W. *YoMaHa'07: Velocity Data Assessed from Trajectories of Argo Floats at Parking Level and at the Sea Surface.* IPRC Technical Note 4 (International Pacific Research Center, 2007).
20. Firing, E., Wijffels, S. E. & Hacker, P. Equatorial subthermocline currents across the Pacific. *J. Geophys. Res.* **103,** 21413–21423 (1998).
21. Ponte, R. M. & Luyten, J. R. Deep velocity measurements in the western equatorial Indian Ocean. *J. Phys. Oceanogr.* **20,** 44–52 (1990).
22. d'Orgeville, M., Hua, B. L. & Sasaki, H. Equatorial deep jets triggered by a large vertical scale variability within the western boundary layer. *J. Mar. Res.* **65,** 1–25 (2007).
23. Hua, B. L. *et al.* Destabilization of mixed Rossby gravity waves and the formation of equatorial zonal jets. *J. Fluid Mech.* **610,** 311–341 (2008).
24. Eden, C. & Dengler, M. Stacked jets in the deep equatorial Atlantic Ocean. *J. Geophys. Res.* **113,** C04003 (2008).
25. McPhaden, M. J., Proehl, J. A. & Rothstein, L. M. The interaction of equatorial Kelvin waves with realistically sheared zonal currents. *J. Phys. Oceanogr.* **16,** 1499–1515 (1986).
26. Brown, G. L. & Sutherland, B. R. Internal wave tunnelling through non-uniformly stratified shear flow. *Atmosphere-Ocean* **45,** 47–56 (2007).
27. Gouretski, V. V. & Koltermann, K. P. *WOCE Global Hydrographic Climatology.* Report 35 (Bundesamt für Seeschifffahrt und Hydrographie, 2004).
28. Cane, M. A. & Moore, D. W. A note on low-frequency equatorial basin modes. *J. Phys. Oceanogr.* **11,** 1578–1584 (1981).
29. Keenlyside, N. S. & Latif, M. Understanding equatorial Atlantic interannual variability. *J. Clim.* **20,** 131–142 (2007).
30. Okumura, Y. & Xie, S.-P. Some overlooked features of tropical Atlantic climate leading to a new Niño-like phenomenon. *J. Clim.* **19,** 5859–5874 (2006).

**Supplementary Information** is linked to the online version of the paper at www.nature.com/nature.

**Acknowledgements** This study was supported by the German Federal Ministry of Education and Research as part of the co-operative project 'North Atlantic' and by the German Science Foundation as part of the Sonderforschungsbereich 754 'Climate-Biogeochemistry Interactions in the Tropical Ocean'. The contribution of J.M.T. was facilitated by support from the Woods Hole Oceanographic Institution's Columbus O'Donnell Iselin Chair for Excellence in Oceanography. We thank J. Fischer for mooring planning and field-work participation, F. Ascani for discussion and S.-H. Didwischus for data processing. This study uses PIRATA velocity and temperature data provided through the TAO project office, Argo float drift data provided by APDRC/IPRC[19], rainfall data from the Global Precipitation Climatology Project, Met Office Hadley Centre and microwave optimally interpolated SST data, NCEP/NCAR reanalysis wind data, and AVISO sea level anomaly data (Supplementary Table 1).

**Author Contributions** P.B. led the project and designed the study including sea-going work and data analysis. A.F. and V.H. processed and analysed moored velocity, Argo float and satellite data. J.M.T. performed moored profiler measurements, its data processing and its analysis. P.B., M.D. and R.J.G. led the drafting of the manuscript. All authors contributed to the interpretation of the results and provided substantial input to the manuscript.

**Author Information** Reprints and permissions information is available at www.nature.com/reprints. The authors declare no competing financial interests. Readers are welcome to comment on the online version of this article at www.nature.com/nature. Correspondence and requests for materials should be addressed to P.B. (pbrandt@ifm-geomar.de).

## METHODS

Surface zonal velocity anomaly at the Equator, averaged between 35° W and 15° W (Fig. 1b), was calculated by applying a second-order fit in latitude to monthly mean meridional sea level anomaly distributions between 1° S and 1° N and evaluating equatorial geostrophy using the obtained curvature. Mean zonal velocities from Argo float drifts between 950 and 1,050 m (Fig. 1b) were derived by removing outliers using a standard-deviation criterion and averaging over time (1-yr period) and space (from 1° S to 1° N and from 35° W to 15° W). The standard error of the nominal 1,000-m zonal velocities (Fig. 1b) was calculated by dividing their standard deviation by the square root of the number of float observations. Monthly time series (Fig. 1b) were filtered using a running annual mean. The dominant period of these time series was estimated by calculating the variance explained by a plane-wave fit (Supplementary Fig. 1).

In the subsurface temperature and velocity time series from PIRATA buoys and subsurface moorings, which are used to produce Fig. 3, data gaps are present. Here monthly time series were derived by monthly averaging and subtracting a mean annual cycle.

Harmonic analyses of zonal velocity and temperature time series (Figs 1b and 3b, c) were performed by fitting the following linear regression model in a least-squares sense to the monthly data:

$$\mathbf{d}_{\mathrm{m}} = g\boldsymbol{\beta} = \beta_1 \mathbf{I}_N + \beta_2 \cos(\omega \mathbf{t}) + \beta_3 \sin(\omega \mathbf{t})$$

Here $\mathbf{t}$ is the time vector corresponding to the data vector, $\mathbf{d}$, both of which are of length $N$; $\cos(\omega\mathbf{t})$ and $\sin(\omega\mathbf{t})$ are the vectors whose elements are the cosines and sines of the elements of $\omega\mathbf{t}$, respectively; $\omega = 2\pi/p$ is the angular frequency, where $p$ is the period; $g$ is the model matrix; $\boldsymbol{\beta}$ is a column vector of scalar model factors ($\beta_1$, $\beta_2$ and $\beta_3$); and $\mathbf{I}_N$ is a vector of length $N$ whose elements all equal 1. The error matrix is given by

$$\Delta\beta = \sqrt{\frac{(g^{\mathrm{T}}g)^{-1}(\mathbf{d}-\mathbf{d}_{\mathrm{m}})^{\mathrm{T}}(\mathbf{d}-\mathbf{d}_{\mathrm{m}})}{n-k}}$$

where $n$ is the number of degrees of freedom and $k = 2$ is the number of dependent model factors. The standard errors of the elements of $\boldsymbol{\beta}$ are given by the diagonal elements of $\Delta\beta$. The degrees of freedom used for the calculation of the standard error of the resulting amplitudes were approximated as the length of the time series divided by a quarter of the deep-jet oscillation period, and are $n = 14$ for ATL3 SST (HadISST), $n = 10$ for ATL3 SST (microwave optimally interpolated SST), $n = 14$ for geostrophic zonal velocity anomaly, $n = 10$ for the Argo float drift data (Fig. 1b and Supplementary Table 2), and $n = 5$ to $n = 7$ for the moored zonal velocity and subsurface temperature data (Fig. 3) varying with depth owing to data gaps. The phase errors (Fig. 3c) are maximum errors derived using the standard errors of the model factors ($\Delta\beta_2$ and $\Delta\beta_3$) by applying linear error propagation for an arbitrary phase lag.

The significance of the correlation (Fig. 1a) is obtained using surface wind and rainfall time series of the same length as the microwave optimally interpolated SST data series (Fig. 1b), which are additionally 270-d low-pass-filtered and have $n = 10$. Sources and periods of all data sets used are given in Supplementary Tab. 1.

Equatorial zonal velocities from 1,000-m Argo float drift data acquired between 1° S and 1° N were plotted as functions of time and longitude in Fig. 4. The data model

$$\mathbf{d}_{\mathrm{m}} = \hat{U}\sin(k\mathbf{x} - \omega\mathbf{t} - \phi\mathbf{I}_N)$$

was applied to the observed zonal velocities. Here $\hat{U}$ is the zonal velocity amplitude, $\sin(k\mathbf{x} - \omega\mathbf{t} - \phi\mathbf{I}_N)$ is the vector whose elements are the sines of the elements of $k\mathbf{x} - \omega\mathbf{t} - \phi\mathbf{I}_N$, $\mathbf{x}$ is the space vector in the zonal direction corresponding to the data vector, $k$ is the zonal wavenumber and $\phi$ is the phase. By maximizing the variance explained by the fit, propagation characteristics of the dominant interannual variability were obtained (Supplementary Fig. 4). In the Atlantic, this fit explains about 28% of the variance of the equatorial zonal velocity from Argo float drift data after subtracting the annual and semi-annual cycles. In the Pacific, the strongest interannual signal (which explains only 8% of the variance) is found at a period of 740 d with a zonal wavelength of $56 \times 10^3$ km. The associated phase velocity corresponds to a first-baroclinic-mode Rossby wave that is very probably forced by the wind (Supplementary Fig. 4). Uncertainties in period and wavelength were estimated by a non-parametric bootstrap procedure where a number of resamples was constructed by random sampling with replacement (Supplementary Fig. 5).

Moored velocity data were acquired using acoustic Doppler current profilers, different single-point current meters and a moored profiler (Figs 2 and 3 and Supplementary Fig. 3). The oceanic variability on short timescales clearly exceeds the measurement accuracy of the different instruments. Owing to a ballasting error, the moored profiler was deployed 'light' and suffered loss of drive-wheel traction over time, resulting in truncation of the down-going profiles as time progressed (Fig. 2).